Electronic Supplementary Material (ESI) for Journal of Materials Chemistry A.
This journal is © The Royal Society of Chemistry 2019

Supporting Information

Construction of highly dispersed mesoporous bimetallic-sulfide nanoparticles locked in N-doped graphitic carbon nanosheets for high energy density hybrid flexible pseudocapacitors

Muhammad Sufyan Javed[a,b], *Hang Lei*[a], *Jinliang Li*[a], *Zilong Wang*[a]*, *Wenjie Mai*[a]*

[a]Siyuan Laboratory, Guangzhou Key Laboratory of Vacuum Coating Technologies and New Energy Materials, Guangdong Provincial Engineering Technology Research Center of Vacuum Coating Technologies and New Energy Materials, Department of Physics, Jinan University, Guangzhou 510632, People's Republic of China

[b]Department of Physics, COMSATS University Islamabad, Lahore Campus, Lahore 54000, Pakistan

Corresponding authors:

E-mail: zilong@email.jnu.edu.cn (Zilong Wang);

wenjiemai@email.jnu.edu.cn (Wenjie Mai)

Table of contents:

1. **Experimental section**
    - **Synthesis of Zn-, Co- and bimetallic (Zn/Co)-MOF nanosheets on carbon cloth**
    - **Synthesis of Zn_xCo_{1-x}-NC@CC**
    - **The sulfide conversion process of bimetallic oxides**
    - **Synthesis of bimetallic MOF-derived mesoporous carbon (MPC)**
2. **Characterization of materials**
    - **Fabrication of single electrode**
    - **Fabrication of ASCs**
    - **Electrochemical measurements and calculations**
3. **Disscussion on negative electrode**
4. **Supporting figures (S1-S14)**
5. **Supporting tables (T1-T2)**
6. **Supporting references**

1. Experimental Section

Synthesis of Zn-, Co- and bimetallic (Zn/Co)-MOF nanosheets on carbon cloth

All chemicals and solvents were purchased from Aladdin Chemicals and used as received without further purification. In a typical synthesis of Zn and Co-MOFs, an aqueous solution of Zn $(NO_3)_2.6H_2O$ (30 mL, 3 mmol) or Co $(NO_3)_2.6H_2O$ (30 mL, 3 mmol) and 2-methylimidazole ($C_4H_6N_2$, 10 mL, 12mmol) were prepared separately. After that, the solution of 2-methylimidazole was quickly injected into Zn $(NO_3)_2.6H_2O$ solution for Zn-MOF and into Co $(NO_3)_2.6H_2O$ solution for Co-MOF, and transferred to 50 mL stainless steel autoclave. A piece of well cleansed CC substrate was immersed and aligned with the wall of the autoclave. The back and upper side of CC was protected by polytetrafluoroethylene type. The autoclaves were incubated at 30, 60 and 100 ^oC for 12 hours and after cooling to room temperature the CC substrates were taken out ant, cleaned with deionized water and ethanol, and dried at 60 ^oC overnight. The molar ratio of Zn^{+2}/Co^{+2} in bimetallic MOFs was adjustable over a wide range by varying the initial metallic precursor ratio. The total molar ratio in bimetallic MOFs was fixed to be 3 mmol during the synthesis. A series of bimetallic MOFs were prepared and categorized as Zn_xCo_{1-x}-MOF, where x/1-x represents the corresponding initial molar ratio of Zn^{+2}/Co^{+2} and obtained bimetallic MOFs are denoted as $Zn_{0.0}Co_{1.0}$-MOF, $Zn_{0.25}Co_{0.75}$-MOF, $Zn_{0.5}Co_{0.5}$-MOF, $Zn_{0.25}Co_{0.75}$-MOF, and $Zn_{1.0}Co_{0.0}$-MOF, respectively. The morphology of the bimetallic MOFs was tuned by varying the reaction temperature, while reaction time was kept constant.

Synthesis of Zn_xCo_{1-x}-NC@CC

The as-synthesized Zn_xCo_{1-x}-MOFs@CC were annealed at 400 ^oC for 2 hours with a ramp rate of 2 ^oC min^{-1} in a nitrogen atmosphere. After cooling down the samples were further sintered at 350 °C with a ramp rate of 2 °C min^{-1} for 1 h to convert it corresponding oxides and denoted as $Zn_xCo_{1-x}O_4$@CC.

The sulfide conversion process of bimetallic oxides

In the subsequent typical sulfidation process, the piece of $Zn_xCo_{1-x}O_4$@CC was placed in a methanol solution of Thioacetamide (TAA) 1.0, 2.5 and 5 mmol, respectively and heated at 120 °C for 2 hours. The as-prepared $Zn_xCo_{1-x}S$@CC were washed with deionized water, ethanol and dried at 60 °C overnight. Finally, the obtained products were annealed under nitrogen at 400 °C for 2 h to get well crystalline phase.

Synthesis of bimetallic MOF-derived mesoporous carbon (MPC)

Bimetallic ($Zn_{0.5}Co_{0.5}$) MOF derived mesoporous carbon (MPC) was synthesized from direct carbonization of zeolitic imidazolate framework ($Zn_{0.5}Co_{0.5}$-MOF). $Zn_{0.5}Co_{0.5}$-MOF was prepared according to the above-mentioned procedure without CC substrate by dual solvent (2:8 water/ethanol) at room temperature. The sample was heated in a tube furnace under a nitrogen atmosphere as follow. First, the temperature was increased up to 200 °C with a ramp rate of 5 °C min^{-1} and was kept constant for 2 h to remove the absorbed water and methanol. The temperature was elevated to 800 °C and remained constant for 4 h. Finally, the sample was dispersed into 2 M HCl solution to remove the residual metal ions and dried at 65 °C for 24 h for further use. The experiment was performed twice to confirm the reproducibility of the used procedure.

2. Characterization of materials

X-ray diffraction (XRD) was acquired with a Rigaku, MiniFlex600, CuK*a* radiation (λ = 1.54065 Å). The X-ray Photoelectron Spectroscopy was carried out using XPS, Ulvac-Phi, PHI X-tool. Surface morphologies of the products were examined by field emission scanning electron microscopy (SEM, ZEISS ULTRA 55) and transmission electron microscopy (TEM, JEOL 2100F, 200 kV) equipped with an energy dispersive X-ray spectrometer (EDS). The elemental contents were recorded by inductively coupled plasma atomic emission spectrometry (ICP-AES, X Series 2). The BET specific surface area was determined using N_2 adsorption/desorption isotherm measurements by multipoint Brunauer-Emmett-Teller (BET) method with Quantachrome Instrument (version 5.12) and pore size distribution was computed by Barret-Joyner-Halenda (BJH) method.

Fabrication of single electrode

$Zn_xCo_{1-x}O$-NC@CC and $Zn_xCo_{1-x}S$-NC@CC were cut into 1×1 cm^2 and directly used as electrodes without any polymer binder and conductive additives for ASCs. The mass loading density was about 1.03 and 1.20 mg cm^{-2} for $Zn_xCo_{1-x}O$-NC@CC and $Zn_xCo_{1-x}S$-NC@CC, respectively, which was carefully calculated by the difference between pristine and growth of active materials on CC. For simplicity we denote the $Zn_{0.76}Co_{0.24}O_4$-NC@CC with ZCO-NC and $Zn_{0.76}Co_{0.24}S$-NC@CC with ZCS-NC-II.

Fabrication of ASCs

Solid-state hybrid SCs were fabricated using ZCS-NC-II as a positive electrode and MPC as a negative electrode with LiCl/PVA solid-state electrolyte and a piece of Whatman filter paper (8 μm thickness). The LiCl/PVA solid-state electrolyte was prepared by mixing 12.6 g LiCl and 6 g PVA in 60 mL deionized water and heated at 85 ^oC until the mixture became the clear homogenous solution. The LiCl/PVA was constantly stirred for 2 h at room temperature to remove the air bubbles. The negative electrode was first prepared by mixing the MPC (90 %) and Polyvinylidene fluoride (PVDF) (10 %) in N-Methyl-2-pyrrolidone (NMP) and stirred until the mixture has become homogenous. The obtained mixture was pasted on the CC and dried at 60 ^oC prior to use. In order to obtain optimum performance of hybrid solid state SC device, the mass of positive and negative electrodes were optimized according to the charge balance equation, i.e. $q^+ = q^-$, where q is the charge and can be calculated using $q = m\,C\,V$. Thus, $m_+/m_- = (C_-V_-) / (C_+V_+)$. Based on the calculation, the optimal mass loading ratio between ZCS-NC-II and MPC was 0.346.

Electrochemical Measurements and calculations

The electrochemical measurements of single electrodes were conducted in a three-electrode system using LiCl as an aqueous neutral electrolyte, Ag/AgCl as a reference electrode, and a platinum plate as a counter electrode. Cyclic Voltammetry (CV) and galvanostatic charge/discharge (GCD) tests for both two and three electrode systems were recorded using electrochemical workstation (CHI 660E, China). Electrochemical impedance spectroscopy (EIS) measurements were investigated under A.C. signal of voltage (5 mV) in the frequency range of 0.01-100 kHz. Each electrochemical test in three and two electrode systems was performed three times to confirm the reproducibility of the results. The specific capacitance in three-electrode system (C_s), specific capacitance in two electrode system (C_{cell}), energy density (E), power density (P), coulombic efficiency (η) and energy efficiency (E_{ff}) of hybrid SC device were computed based on the total mass of the both electrode materials using the following equations [1-2].

$$C_s = \frac{\int I\,dt}{m\left(\mathrm{V_f} - \mathrm{V_i}\right)} \tag{1}$$

$$C_a = \frac{\int I\,dt}{A\left(\mathrm{V_f} - \mathrm{V_i}\right)} \tag{2}$$

$$C_{cell} = \frac{\int I\,dt}{M\left(\mathrm{V_f} - \mathrm{V_i}\right)} \tag{3}$$

$$C_{(a)cell} = \frac{\int I\,dt}{S\left(\mathrm{V_f} - \mathrm{V_i}\right)} \tag{4}$$

$$E = \frac{\int I\,dt}{M \times 3.6} \qquad (5)$$

$$P = \frac{E}{\Delta t_d} \times 3600 \qquad (6)$$

Where, C_s, C_{cell} ($F\,g^{-1}$) and C_a $C_{a\,(cell)}$ ($F\,cm^{-2}$) are the specific and areal capacitance of single electrode and ZCS//MPC-ASC, respectively; $\int I\,dt$ is the area under discharge curve; m (g) is the mass of active material on single electrode; A (cm^2) is the area of the working electrode; $\Delta V = V_\mathrm{f} - V_\mathrm{i}$ is the potential window; S is the working area of the ZCS//MPC-ASC; M (g) is the total mass of positive and negative electrode materials; P ($W\,kg^{-1}$) is the power density; E ($Wh\,kg^{-1}$); Δt_d is the discharging time (s).

Calculation of capacity from capacitacnce:

Capacity (mAh g^{-1}) = Capacitance (F g^{-1}) × Potential Window (V) × $\left(\frac{1000}{3600}\right)$

Or

Capacity (mAh g^{-1}) = Capacitance (F g^{-1}) × Potential Window (V) × 0.277

3. Disscussion on negative electrode

The SEM images of the MPC polyherans are shown in Figure S11, and corresponding physical characterizations XRD, XPS and BET/BJH pore size distribution are demonstrated in S12 and S13, respectively. These characterizations confirm the existance of pure MPC without any impurity. The electrochemcial performance of MPC in LiCl aqeous electrolyte is shown in Figure S14 to optimize the ZCS-NC//MPC-ASC performance. The MPC electrode revealed the high capacitance of 400 F/g at 1 A/g with high capacitance retention ~100 after 5000.

4. Supporting Figures

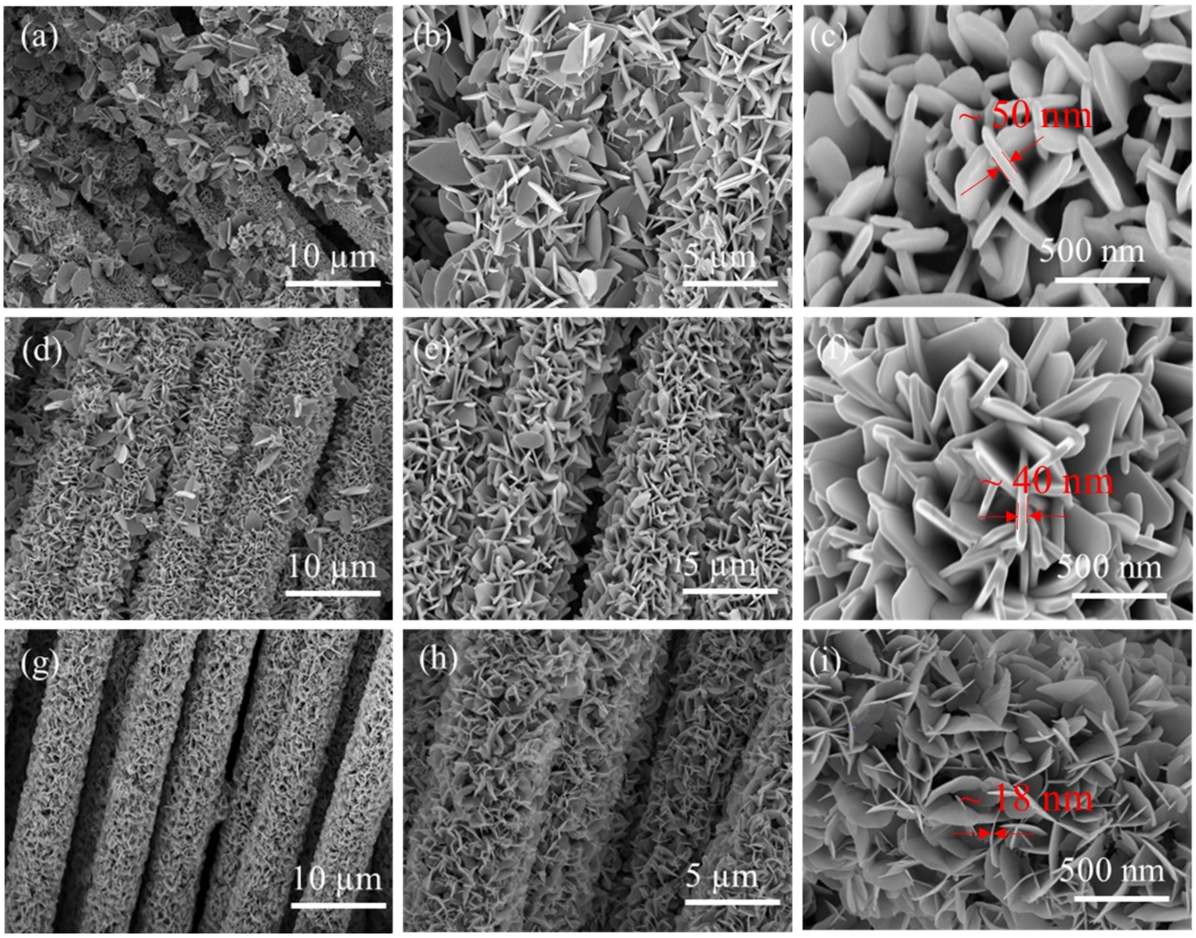

Figure S1: Low and high-resolution FE-SEM images of ZCO-NC@CC precursor; (a-c) as-synthesized product at room temperature for 12 h, (d-f) as-synthesized product at 60 °C for 12 h, (g-i) as-synthesized product at 100 °C for 12 h.

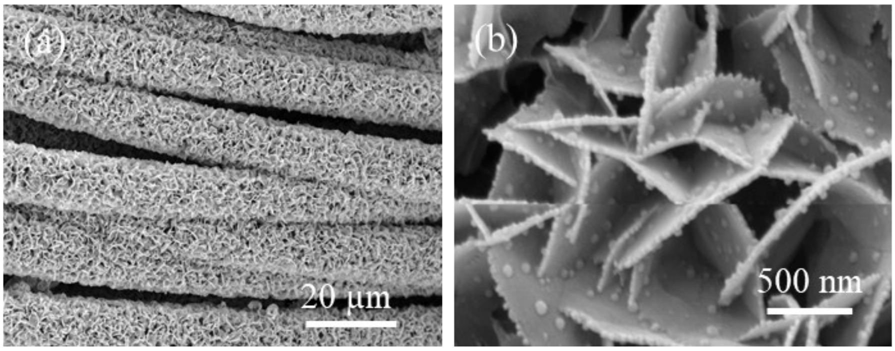

Figure S2: Low and high-resolution FE-SEM images of ZCS-NC-I after thermal treatment at 400 ^oC for 2h in N_2 atmosphere.

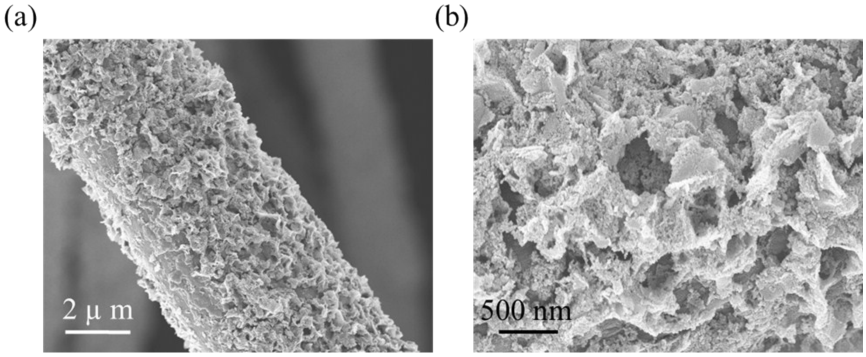

Figure S3: Low and high-resolution FE-SEM images of ZCS-NC-III after thermal treatment at 400 ^oC for 2h in N_2 atmosphere.

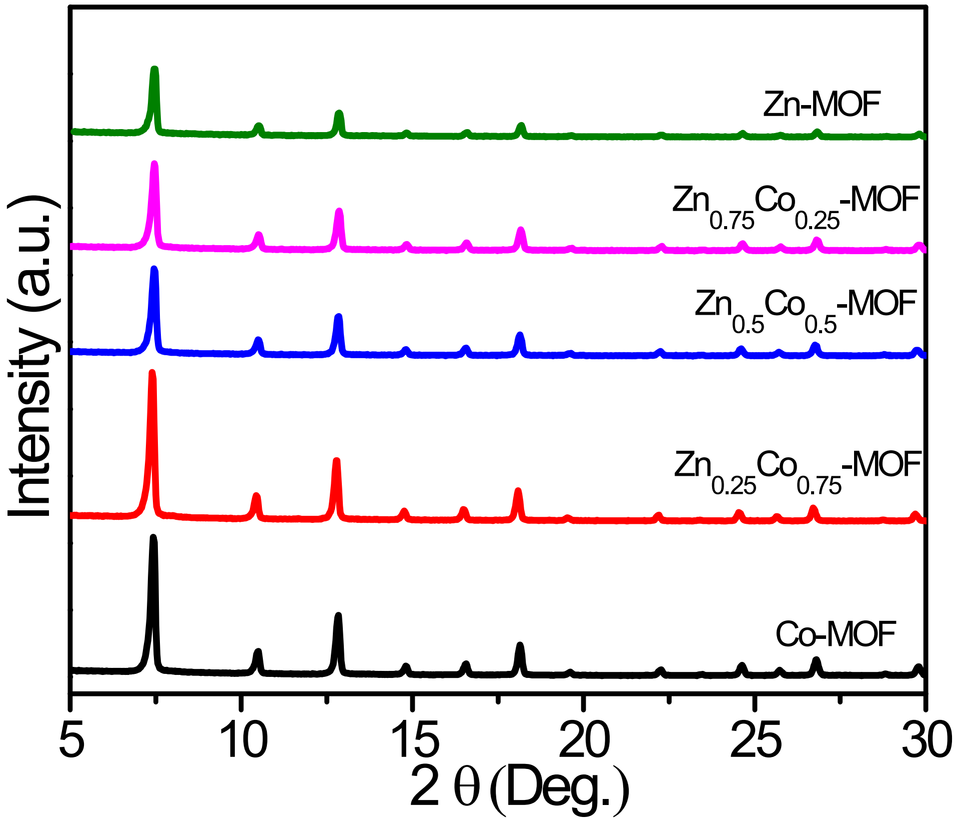

Figure S4(a): XRD patterns of as-synthesized bimetallic MOFs with different feeding ratios of Zn and Co.

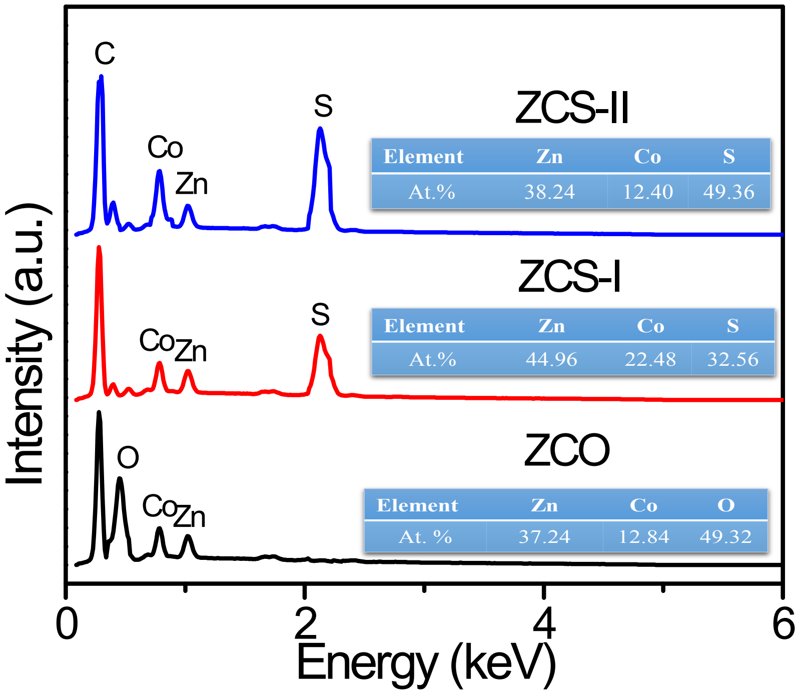

Element	Zn	Co	S
At.%	38.24	12.40	49.36

Element	Zn	Co	S
At.%	44.96	22.48	32.56

Element	Zn	Co	O
At. %	37.24	12.84	49.32

Figure S4(c): EDS analysis of ZCO-NC@CC, ZCS-NC@CC-I, and ZCS-NC@CC-II.

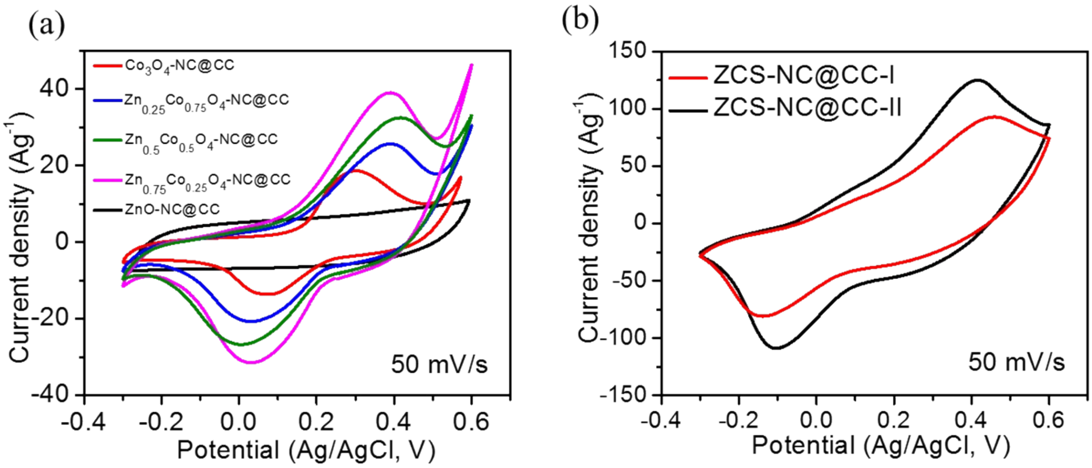

Figure S5: (a) Optimization of the electrochemical performance of ZCO-NC electrode in aqueous electrolyte using different feeding ratios of Zn and Co. (b) Optimization of the electrochemical performance of ZCS-NC electrode in the aqueous electrolyte with low and high sulfurization contents.

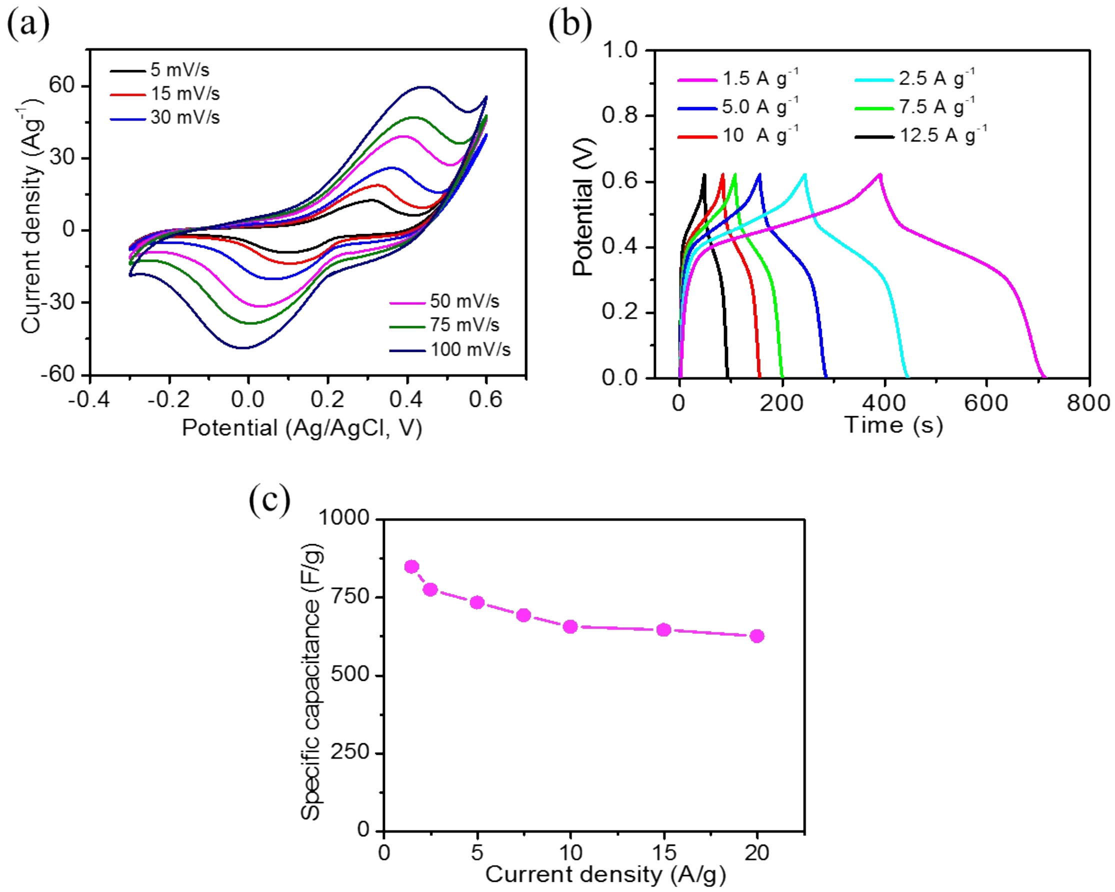

Figure S6: (a-b) CV and GCD curves of $Zn_{0.76}Co_{0.24}O_4$-NC in the aqueous electrolyte at various scan rates and current densities, respectively. (c) The specific capacitance of $Zn_{0.76}Co_{0.24}O_4$-NC electrode as a function of current density.

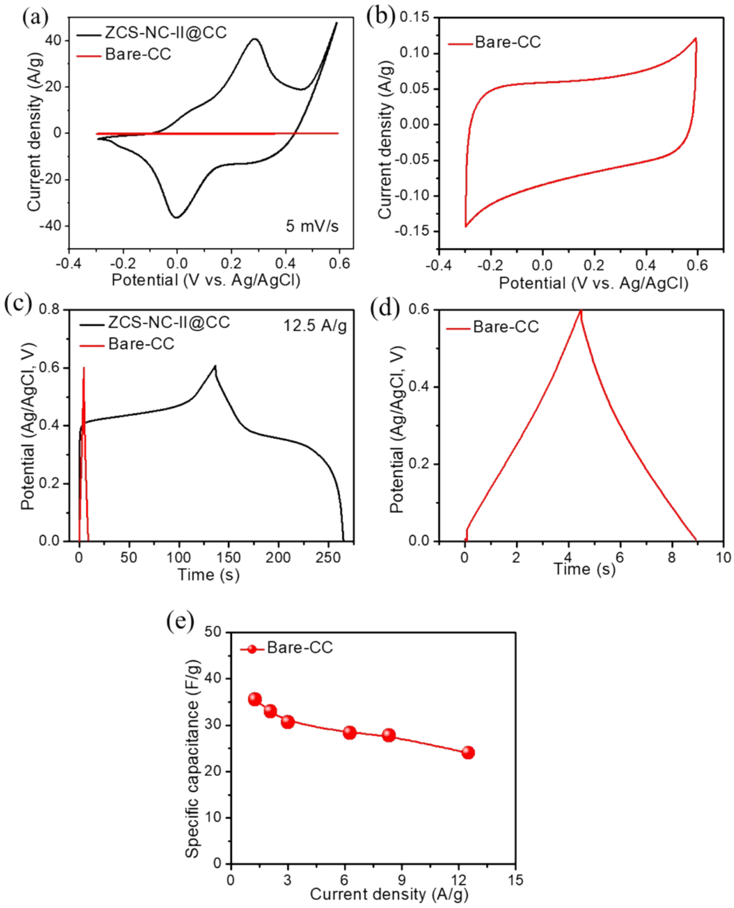

Figure S7: Electrochemical performance of bare-CC substrate: (a) Comparative CV curves, (b) Magnified CV curve of bare-CC substrate, (c) Comparative GDC curves, (d) Magnified GCD curve of bare-CC substrate, (e) Specific capacitance as a function of current density.

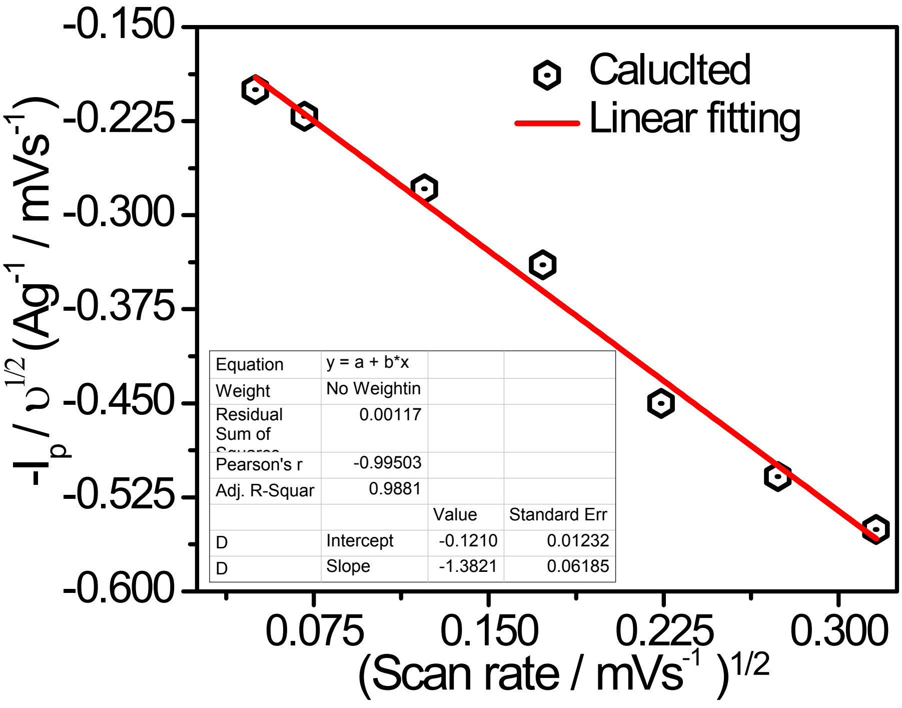

Equation	y = a + b*x		
Weight	No Weightin		
Residual Sum of	0.00117		
Pearson's r	-0.99503		
Adj. R-Squar	0.9881		
		Value	Standard Err
D	Intercept	-0.1210	0.01232
D	Slope	-1.3821	0.06185

Figure S8: Relationship between (peak current/scan rates) versus square root of scan rate for the determination of k_1 and k_2 constants.

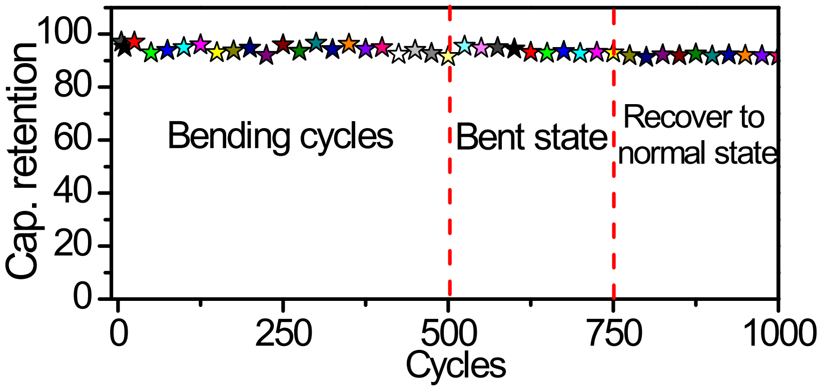

Figure S9: Capacitance retentation of ZCS-NC//MPC-ASC during the 500 bending cycles and kept at bent sate for 250 cycles, and 250 cycles after recovering to its tormal state.

Figure S10: The digital photograph of thickness measurements for ZCS-NC//MPC-ASC (including qelectrodes, ausi-solid-state gel electrolyte and separator).

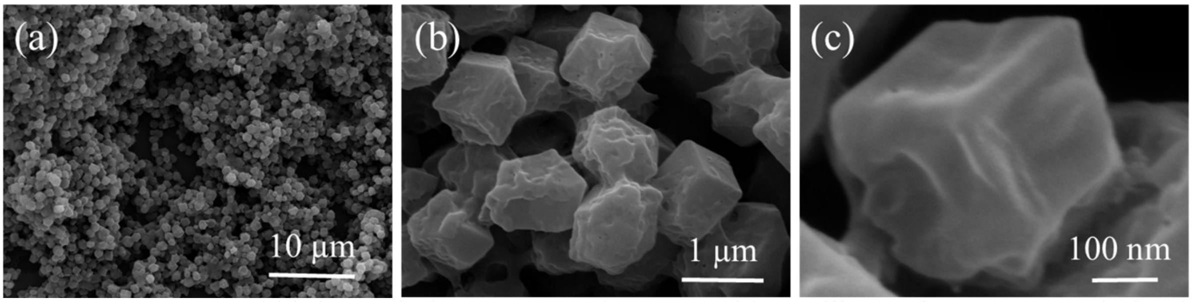

Figure S11: Low and high-resolution FE-SEM images of bimetallic (Zn/Co: 1) MOF derived nitrogen-doped mesoporous carbon.

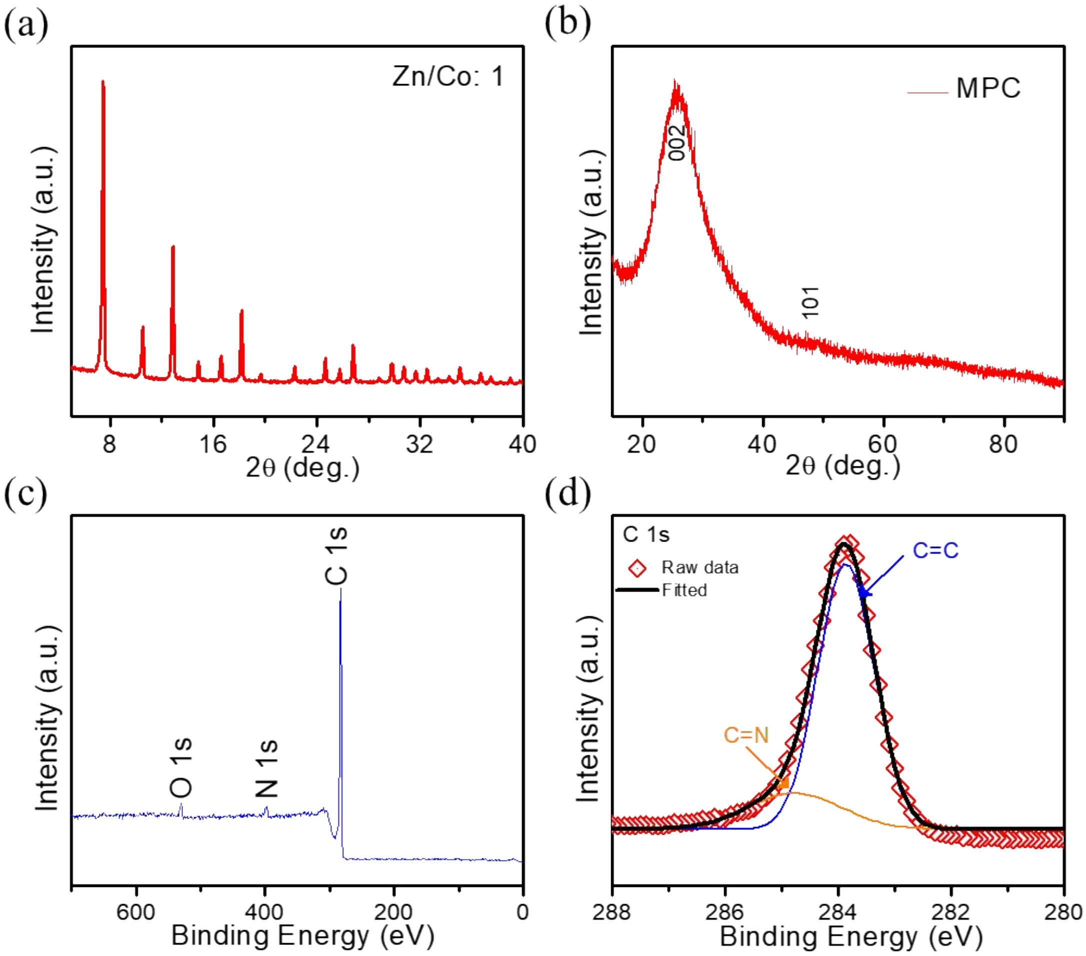

Figure S12: (a) Physical characterization of bimetallic (Zn/Co: 1) MOF precursor and MOF derived nitrogen-doped mesoporous carbon. (a) XRD pattern of MOF precursors, (b) MOF derived nitrogen-doped mesoporous carbon, (c) XPS full survey and (d) De-convoluted XPS spectrums of C 1s.

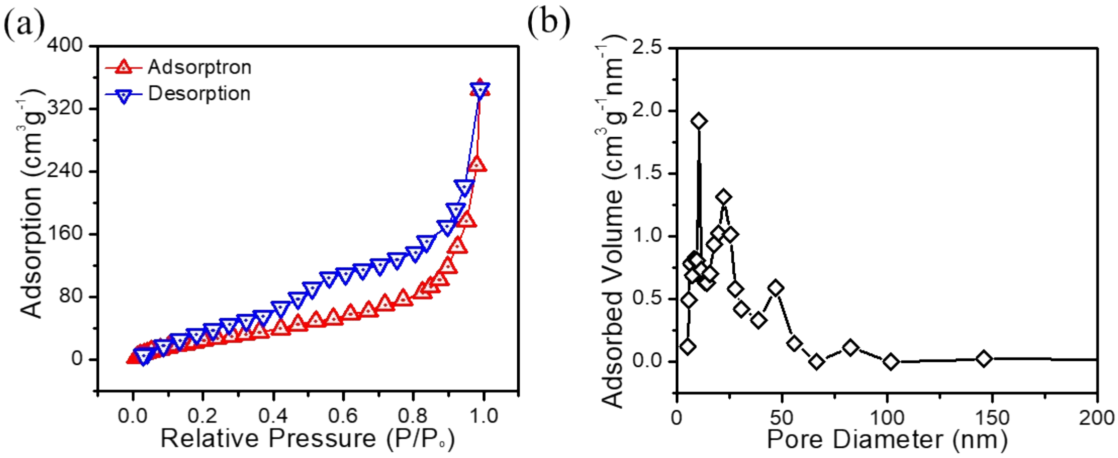

Figure S13. (a) N_2 adsorption-desorption isotherms and (b) pore size distribution curve derived using BJH method for MOF derived nitrogen-doped mesoporous carbon.

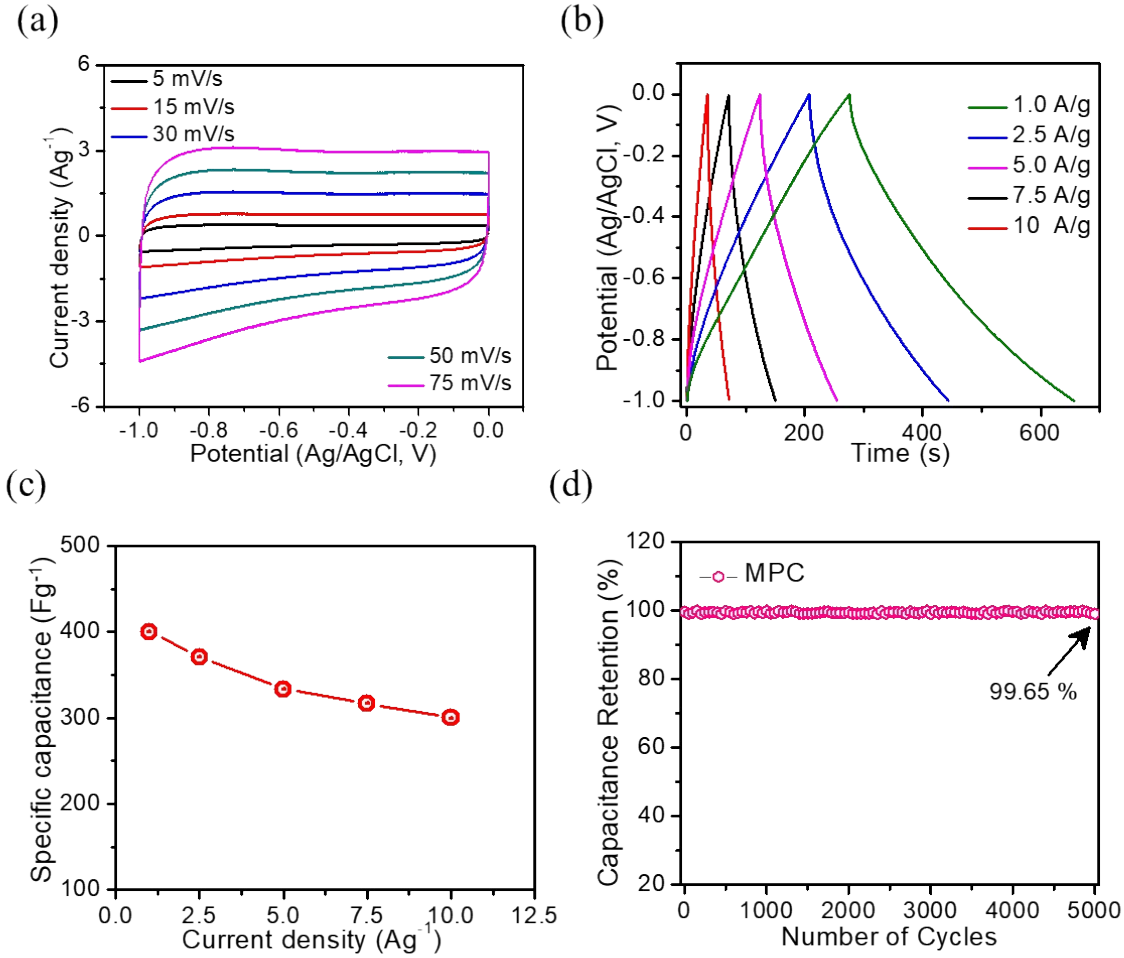

Figure S14. Electrochemical performance of bimetallic (Zn/Co: 1) MOF derived nitrogen-doped mesoporous carbon in aqueous electrolyte. (a) CV cures in potential window of -1.0 to 0.0 V at various scan rates, (b) GCD curves in potential window of -1.0 to 0.0 V at various current densities, (c) specific capacitance as a function of current density and (d) capacitance retention versus number of cycles.

5. Supporting Tables

Table T1: The atomic percentages of Zn, Co and S elements in ZCO-NC, ZCS-NC-I and ZCS-NC-II were also examined by inductively coupled plasma optical emission spectroscopy (ICP-OES)

Samples	Zn [at. %]	Co [at. %]	S [at. %]	O [at. %]
$Zn_{0.76}Co_{0.24}O_4$-NC	27.9	13.6	-	54.7
$Zn_{0.76}Co_{0.24}S$-NC-I	32.75	9.86	38.74	18.65
$Zn_{0.76}Co_{0.24}S$-NC-II	29.78	10.20	45.63	14.39

Table T2: The comparison of the ZCS-NC-II based single electrode and full solid state supercapacitor with previous literatures, where we denote C_{SS} for Specific Capacitance (Single electrode), C_{ST} for Specific Capacitance (two electrode device), *v* for scan rate, *n* for cycle numbers (Single electrode), *E* for Energy density and *P* for Power density (two electrode device).

No	Materials	C_{SS} (F g^{-1}) at *v* (mVs^{-1})	C_{ST} (F g^{-1}) at *v* (mVs^{-1})	*E* (Wh kg^{-1})	*P* (W kg^{-1})	Stability (%) after *n*	Ref./year
0	$Zn_{0.76}Co_{0.24}S$-NC	2168.75 at 1.25 A/g	260.58 at 1 A/g	**92.59**	846.02	95.6, 10000	This work
1	Zn-Co-S nanosheets	2354 at 0.5 A/g	197 at A/g	**31.9**	8500	88.6, 1000	[3]/2018
2	Zn-Co-S nanowires	733 at 3 mAcm^{-2}	102 at 3 mAcm^{-2}	**81.6**	559.2	92.1, 10000	[4]/2018
3	Zn-Co-S@$Ni(OH)_2$	2156 at 1 A/g	319 at 1 A/g	**74.93**	650	94, 3000	[5]/2018
4	Zn-Co-S nanosheets	2484 at 2 A/g	150 at 0.5 A/g	**50.2**	388	99, 1000	[6]/2016
5	Zn-Co-S nanostructures	486.2 at 2 A/g	-	**-**	-	86.4, 2000	[7]/2015
6	$Co_{0.33}Fe_{0.67}S_2$ nanoparticles	310.2 at 2 mVs^{-1}	187.8 at 2 mVs^{-1}	**66.8**	300.5	102, 10000	[8]/2018
7	Ni-Co-S nanosheets	1406.9 at 0.5 A/g	-	**24.8**	850	88.6, 1000	[9]/2018
8	Zn-Co-S cages	1266 at 1 A/g	-	**-**	-	91, 10000	[10]/2017
9	Mn-Co-S nanostructures	1402 at 1 A/g	121 at 1 A/g	**43**	801	95, 5000	[11]/2017
10	Fe-Co-S naosheets	2411 at 3 mAcm^{-2}	214 at 5 mAcm^{-2}	**76**	755	92.2, 5000	[12]/2017
11	Cu-Co-S nanowires	2163 at 3 mAcm^{-2}	124 at 24 mAcm^{-2}	**44.1**	800	94, 6000	[13]/2016

6. Supporting References

[1] P. Yang and W. Mai, *Nano Energy*, 2014, **8**, 274-290.

[2] L. Du, P. Yang, X. Yu, P. Liu, J. Song and W. Mai, *Journal of Materials Chemistry A*, 2014, **2**, 17561-17567.

[3] K. Tao, X. Han, Q. Cheng, Y. Yang, Z. Yang, Q. Ma and L. Han, *Chemistry–A European Journal*, 2018, **24**, 12584-12591.

[4] C. Li, J. Balamurugan, N. H. Kim and J. H. Lee, *Advanced Energy Materials*, 2018, **8**, 1702014.

[5] J. A. Syed, J. Ma, B. Zhu, S. Tang and X. Meng, *Advanced Energy Materials*, 2018, **8**, 1800106.

[6] H. Tong, W. Bai, S. Yue, Z. Gao, L. Lu, L. Shen, S. Dong, J. Zhu, J. He and X. Zhang, *Journal of Materials Chemistry A*, 2016, **4**, 11256-11263.

[7] J. Yang, Y. Zhang, C. Sun, G. Guo, W. Sun, W. Huang, Q. Yan and X. Dong, *Journal of Materials Chemistry A*, 2015, **3**, 11462-11470.

[8] W. Liu, H. Niu, J. Yang, K. Cheng, K. Ye, K. Zhu, G. Wang, D. Cao and J. Yan, *Chemistry of Materials*, 2018, **30**, 1055-1068.

[9] K. Tao, X. Han, Q. Ma and L. Han, *Dalton Transactions*, 2018, **47**, 3496-3502.

[10] P. Zhang, B. Y. Guan, L. Yu and X. W. Lou, *Angewandte Chemie*, 2017, **129**, 7247-7251.

[11] A. M. Elshahawy, X. Li, H. Zhang, Y. Hu, K. H. Ho, C. Guan and J. Wang, *Journal of Materials Chemistry A*, 2017, **5**, 7494-7506.

[12] S. Tang, B. Zhu, X. Shi, J. Wu and X. Meng, *Advanced Energy Materials*, 2017, **7**, 1601985.

[13] S. E. Moosavifard, S. Fani and M. Rahmanian, *Chemical Communications*, 2016, **52**, 4517-4520.